

Quarterly Report  
for the Period Ending March 31, 2002  
“Practical Superconductor Development for Electrical Power Applications”

Principal Investigator

U. Balachandran

April 2002

**PRACTICAL SUPERCONDUCTOR DEVELOPMENT  
FOR ELECTRICAL POWER APPLICATIONS  
ARGONNE NATIONAL LABORATORY  
QUARTERLY REPORT FOR THE PERIOD ENDING MARCH 31, 2002**

This is a multiyear experimental research program that focuses on improving relevant material properties of high- $T_c$  superconductors (HTSs) and developing fabrication methods that can be transferred to industry for production of commercial conductors. The development of teaming relationships through agreements with industrial partners is a key element of the Argonne National Laboratory (ANL) program.

### **Technical Highlights**

The capabilities and performance of a new pulsed laser deposition system (PLD2) are described. Using PLD2, a  $YBa_2Cu_3O_x$  (YBCO) film with critical current density ( $J_c$ ) of  $5.3 \text{ MA/cm}^2$  was prepared on single-crystal  $SrTiO_3$  (STO). Study of a RABiTS<sup>TM</sup> sample from Oak Ridge National Laboratory showed new effects of magnetic history on grain boundary transport in YBCO. The critical current ( $I_c$ ) of melt-textured YBCO rings was measured under pulsed current conditions.

### **New Pulsed Laser Deposition System**

A new pulsed laser deposition system (PLD2) with a Lambda Physik LPX210i excimer laser, shown in Fig. 1, was designed and constructed. This system was used to fabricate high-quality YBCO thin films on both single-crystal and metallic substrates. With its optical beam-rastering capability and the higher power and frequency of its laser (100 Hz/60 W), this system is expected to produce more uniform films over a broader area. The laser beam in PLD2 is focused on the target by a 100-mm focal-length lens through a coated quartz port on a 16-in. (40-cm) diameter spherical vacuum chamber. To accommodate the need to deposit films at off-normal inclination angles, the heated sample stage can be tilted; the sample stage can also be used with the PLD1 system. The rotating-target carousel can be water-cooled to maintain a decreased target temperature during depositions at high repetition rates. The substrate-to-target distance and sample inclination angle are readily adjustable without breaking vacuum. With a single-speed turbo pump, the base pressure can reach  $1 \times 10^{-5}$  torr in several minutes. The laser spot size at the target is  $12 \text{ mm}^2$ .

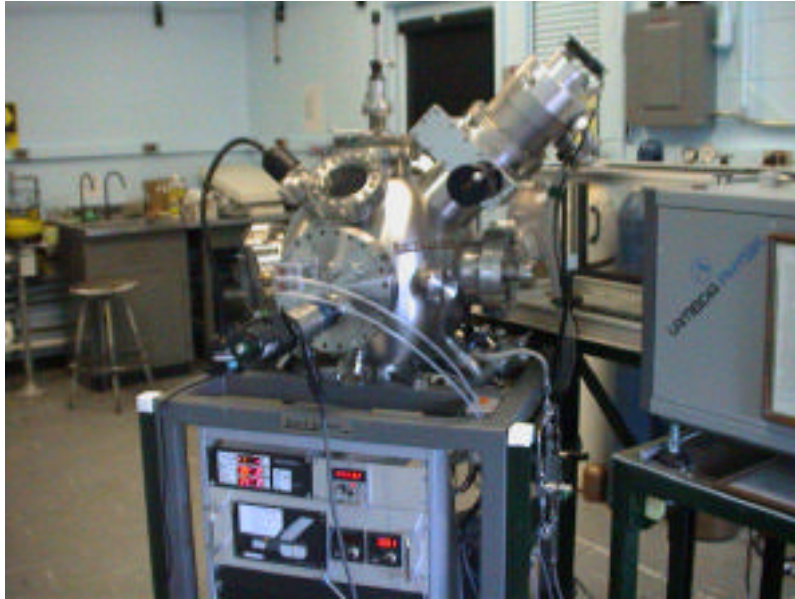


*Fig. 1. New pulsed laser deposition (PLD2) system.*

Improvements provided by the PLD2 system include:

- A more powerful Lambda Physik LPX210i laser, which delivers pulsed laser power up to 60 W at 100 Hz.
- Optical beam-rastering to enhance film uniformity over a broader area.
- A 16-in. (40-cm) diameter spherical vacuum chamber with the potential for adding an ion source for substrate cleaning and ion-beam-assisted pulsed laser deposition.
- A tiltable, heated sample stage, also useable in PLD1, for depositing at a non-zero inclination angle with respect to the laser plume fluence.
- A quadruple variable-speed rotating carousel that carries 2-in. (5-cm) diameter targets and enables multilayer deposition without breaking the vacuum.
- Water-cooled carousel for maintaining a reduced target temperature for depositions with high beam energy and high repetition rate.
- Substrate-to-target distance and substrate inclination angle that can be readily adjusted without breaking the vacuum.
- Dual mass flow controller that allows accurate measurement and control of the gas in-flow and chamber pressure during deposition.

Table 1 lists typical conditions for ablation of YBCO using the PLD2 system. High-quality YBCO films have been deposited on polished, (001)-oriented, single-crystal STO substrates at repetition rates from 8 to 70 Hz. A sharp superconducting transition was observed with a  $T_c(\text{onset})$  of 91.5 K.  $T_c$  showed no noticeable dependence on the repetition rate. Figure 2 shows the current-voltage (I-V) curve for a sample made with a repetition rate of 30 Hz and with dimensions of  $0.27 \mu\text{m} \times 4 \text{ mm} \times 10 \text{ mm}$ . It had a transport  $I_c$  of 46 A and a  $J_c$  of  $5.3 \times 10^6 \text{ A/cm}^2$ . Figure 3a shows the sharp (00l) peaks that are observed in the 2 $\theta$  X-ray diffraction (XRD) pattern from YBCO deposited on STO at 780°C in 200 mtorr flowing oxygen at a repetition rate of 10 Hz. Figure 3b shows the (113)  $\omega$ -scan for YBCO, which gave an average full-width at half-maximum (FWHM) of 0.3°.

Table 1. Conditions used for epitaxial growth of YBCO by PLD2

Laser wavelength	248 nm (Kr-F)
Repetition rate	8-70 Hz
Pulse width	25 ns
Energy density	1 - 2 J/cm <sup>2</sup>
Substrate temperature	700 - 800°C
Operating pressure	100 - 300 mtorr
Oxygen flow rate	1 - 30 sccm
Target-to-substrate distance	4 - 8 cm
Substrate inclination angle	0 - 55°

### Epitaxial Growth of Buffer Layers by PLD

Inclined substrate deposition (ISD) is a promising approach for fabricating biaxially textured template layers on nontextured metallic substrates for YBCO-coated conductors. Compared to ion-beam-assisted deposition (IBAD), ISD is faster, simpler, and easier to perform, and it needs no assisting ion source to develop the biaxial alignment. Unlike the rolling-assisted biaxially textured substrate (RABiTS) approach, which requires complicated high-temperature annealing treatments, ISD yields biaxially textured template films on nontextured metallic substrates at room temperature; consequently, ISD is more robust and less sensitive to heat treatment conditions.

MgO template layers were fabricated on polished Hastelloy C276 (HC) tapes by the ISD approach using electron-beam (e-beam) evaporation. Because the lattice mismatch between YBCO and MgO is large ( 9%), direct deposition of YBCO on the ISD MgO layer does not lead to good superconducting properties. After testing various

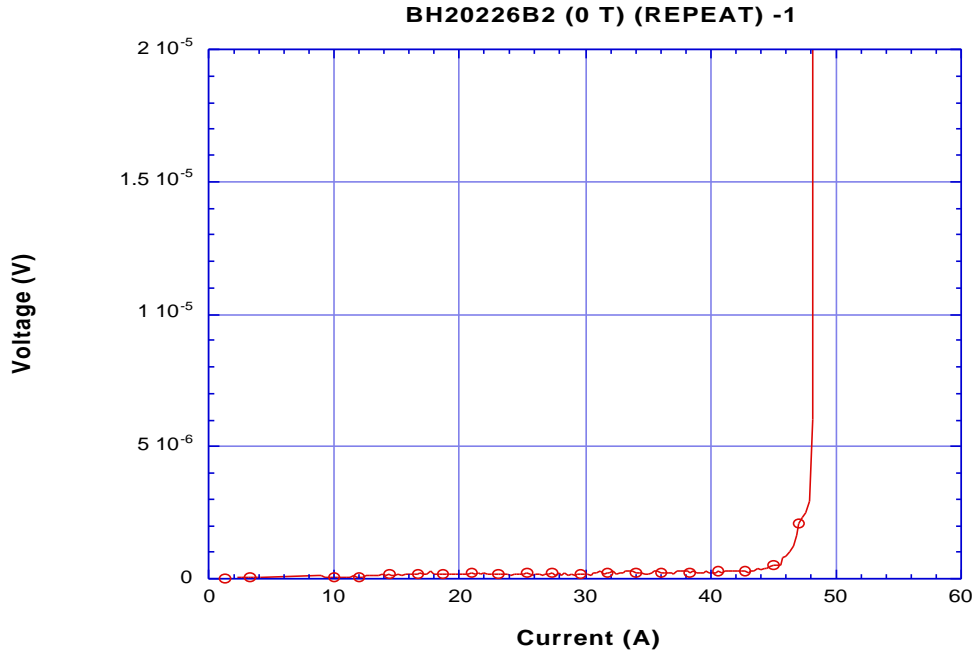


Fig. 2. Zero-field I-V curve of YBCO deposited on SrTiO<sub>3</sub> single-crystal substrate at repetition rate of 30 Hz.

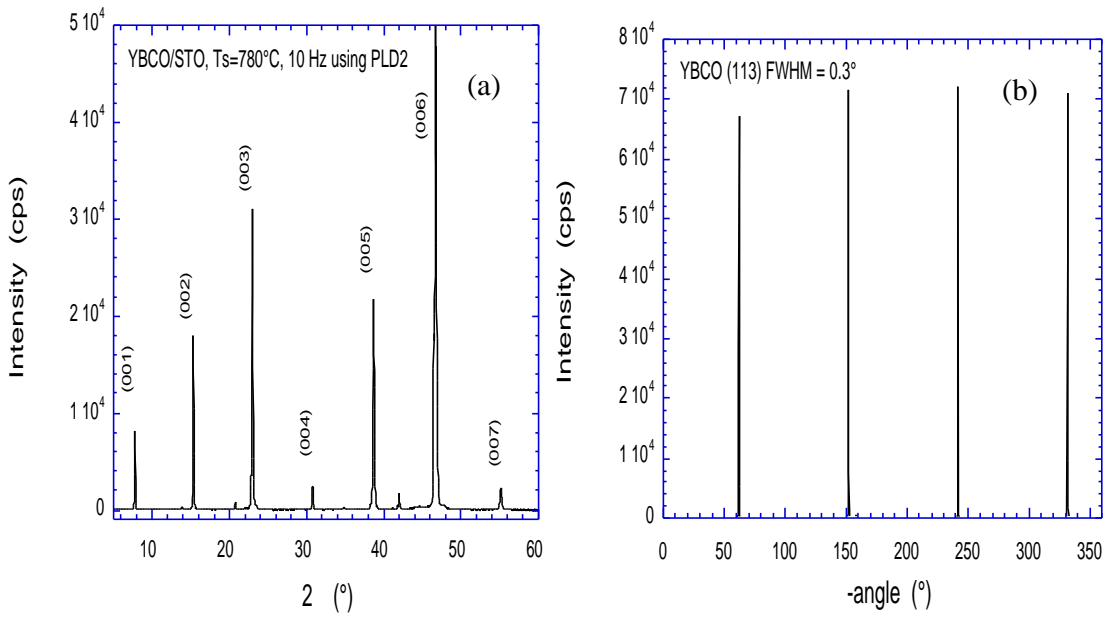


Fig. 3. (a) XRD 2θ and (b) (113) φ-scan patterns for YBCO deposited on SrTiO<sub>3</sub> single-crystal substrate.

buffer layers, we found that good superconductor properties are obtained by depositing epitaxial yttria-stabilized zirconia (YSZ) and  $\text{CeO}_2$  layers on the MgO buffer layer before the YBCO layer is deposited. The layer structure for our approach is illustrated in Fig. 4.

The  $\omega$ -scan for a typical ISD MgO layer has an FWHM of  $10^\circ$ . A cross-sectional scanning electron microscope (SEM) image reveals columnar grains in ISD MgO films, while a plan-view image (Fig. 5) shows a roof-tile structure, in which the c-axis is tilted away from the substrate normal. To reduce surface roughness caused by the roof-tile structure, an additional thin ( $0.5 \mu\text{m}$ ) layer of MgO is epitaxially grown by e-beam evaporation at an elevated temperature. In the following paragraphs, unless otherwise indicated, we refer to both MgO layers together as the ISD MgO layer or MgO buffer layer.

Buffer layers of YSZ and  $\text{CeO}_2$  are being deposited on ISD MgO films by two different techniques. In collaboration with UES, Inc. (Dayton, OH), magnetron sputtering was used to obtain very good biaxial alignment of the YSZ and  $\text{CeO}_2$  layers. Los Alamos National Laboratory has reported that magnetron sputtering also gives good biaxial alignment of YSZ and  $\text{CeO}_2$  on MgO films prepared by IBAD. Magnetron sputtering clearly offers intriguing potential for improving the texture and performance of coated conductors; however, because a magnetron sputtering system is not available at ANL, we are using PLD to grow the YSZ and  $\text{CeO}_2$  layers on ISD MgO films. The conditions that were used for this purpose are listed in Table 2.

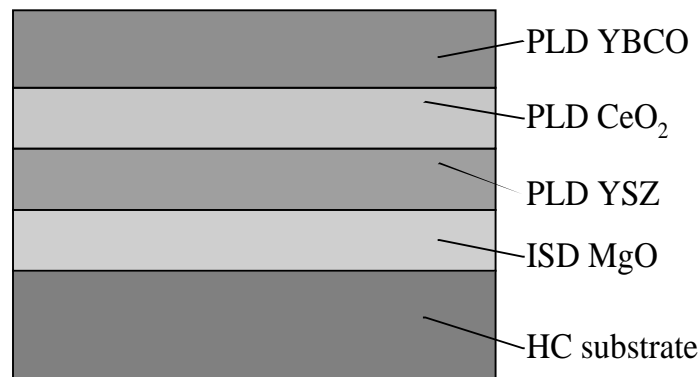


Fig. 4. Layer structure of YBCO deposited on HC substrates by the ISD approach.

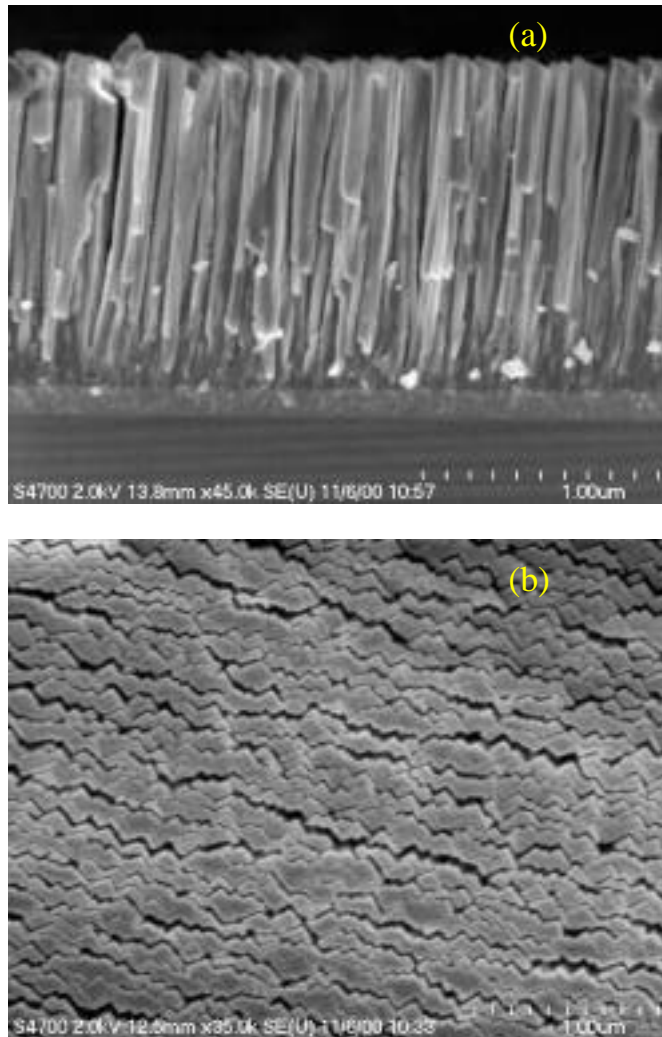


Fig. 5. (a) Cross-sectional and (b) plan-view SEM images of MgO film deposited by ISD using e-beam evaporation.

Table 2. Conditions used for epitaxial growth of YSZ by PLD

Repetition rate	1 - 4 Hz
Laser energy density	1 - 2 J/cm <sup>2</sup>
Substrate temperature	700 - 800°C
Oxygen pressure	1 - 100 mtorr

At a given substrate temperature, the laser repetition rate and oxygen partial pressure in the deposition chamber can significantly affect the texture of YSZ grown on an ISD MgO template layer. Lower repetition rate and reduced oxygen partial pressure in the chamber both help to improve epitaxial growth of the YSZ film. However, a lower repetition rate requires longer deposition time to produce a film with a given thickness. Laser ablation of YSZ at a repetition rate of 2 Hz onto an ISD MgO film heated at 800°C in an atmosphere with 20 mtorr oxygen resulted in good epitaxial growth of the YSZ. Similar conditions can also be used to grow CeO<sub>2</sub> films with good epitaxy. Figure 6 shows the (002) pole figures for the MgO, YSZ, and CeO<sub>2</sub> layers, where the MgO layer was grown by e-beam evaporation (ISD), and PLD was used to grow the YSZ and CeO<sub>2</sub> layers. Good cube-on-cube epitaxy was obtained in both the YSZ and CeO<sub>2</sub> layers. The (002) and (220)  $\phi$ -scans for all three layers are shown in Fig. 7; the FWHMs for the scans were 12° and 16°, respectively.

### Grain Boundary Transport in YBCO Thin Films

We have observed that the history in which the magnetic field is applied has a notable effect on the critical current of YBCO thin-film grain boundaries. The data shown in Fig. 8 were obtained from a single YBCO grain boundary, which we isolated in a RABiTS™ sample (Oak Ridge National Laboratory). These results show additional history dependence beyond our earlier work. Previously, we showed that critical current data from a sample that is cooled to the measurement temperature in the measurement field (FC in Fig. 8) are higher than those from a sample that is cooled to the measurement temperature in zero field before the measurement field is applied (ZFC in Fig. 8).

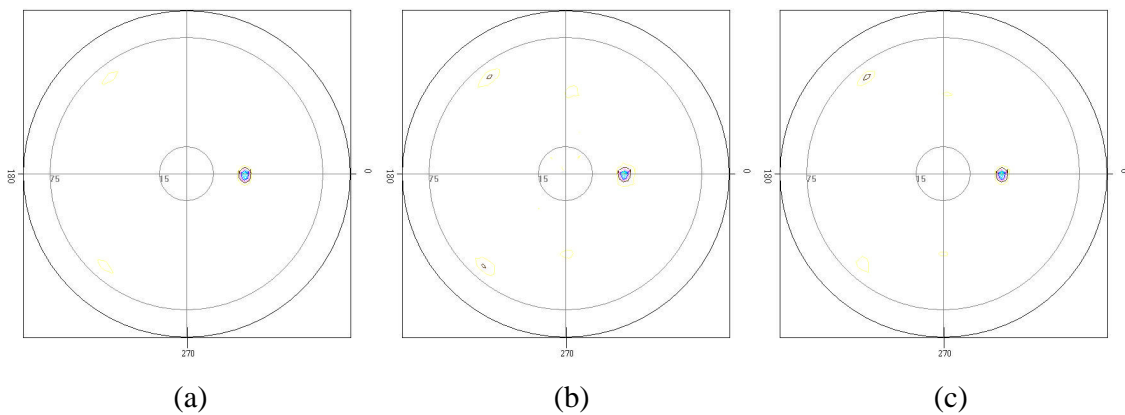


Fig. 6. (002) pole figures for (a) MgO, (b) YSZ, and (c) CeO<sub>2</sub> showing good epitaxial growth of the YSZ and CeO<sub>2</sub> layers.

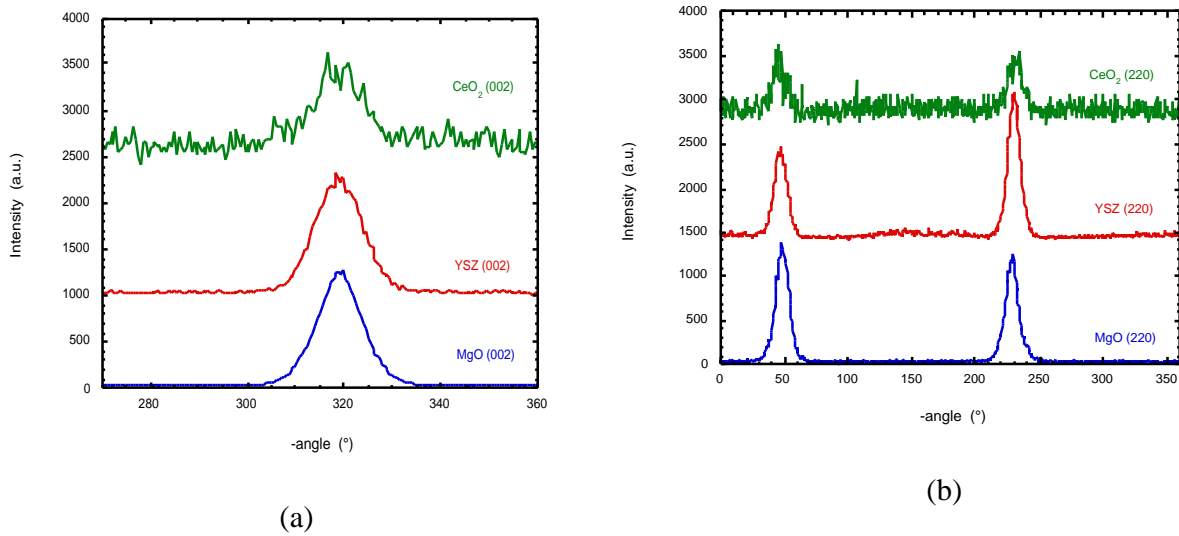


Fig. 7. (a) (002) and (b) (220)  $\omega$ -scans for MgO grown by e-beam evaporation (ISD), and YSZ and CeO<sub>2</sub> grown by PLD.

Our new results reveal that further enhancements can result from field excursions after the sample is field-cooled to the measurement temperature. The data indicate two distinct field regimes. After field-cooling in a modest (50 mT) magnetic field to the measurement temperature (point A in Fig. 8), a significant peak in the critical current data appears upon field-reduction, whereas an increase in the field causes a monotonic reduction in the critical current. A similar peak effect was observed at Oak Ridge during field-reduction from high fields (unpublished data). Near the peak position, the enhancement in critical current over field-cooled values is approximately a factor of two. In contrast, after field-cooling in a low field of several mT (point B in Fig. 8), the critical current drops sharply after either an increase or a decrease in the magnetic field.

The difference between the FC and ZFC measurements can be understood in terms of the different field histories that give rise to distinct flux profiles in the banks near the grain boundary. Apparently, these flux profiles strongly impact the pinning of grain boundary vortices and thus the grain boundary critical currents. This reinforces the importance of the interaction between grain boundary vortices and pinned vortices in the banks of the grain boundary. Similar consideration of the new data may provide further insight into the intriguing physics governing the relationship between the vortex configuration in the banks of grain boundaries and the potential for current transfer across the grain boundaries, and may yield new strategies for improving the performance of the grain boundaries.

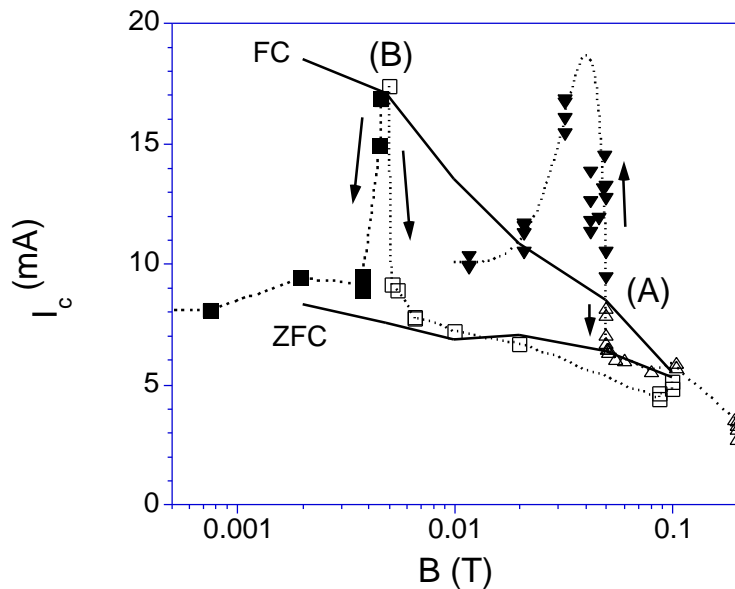


Fig. 8. History dependence of critical current of a YBCO grain boundary in a film grown by the RABiTS<sup>TM</sup> process. Solid lines represent data obtained by field-cooling (FC) and zero-field-cooling (ZFC) to the measurement temperature (77 K). Triangles and squares represent field excursions after field-cooling to 0.05 T (point A) and 0.005 T (point B), respectively. Closed symbols show the effect of decreasing applied field on the critical current; open symbols show the effect of increasing field. The dashed lines are a guide to the eye only.

### Critical Current of YBCO Rings

Several melt-textured YBCO rings were received from Superconductive Components, Inc. (SCI). The dimensions of these rings are:

Minimum inside diameter = 1.60 in. (4.06 cm)

Maximum outside diameter = 2.77 in. (7.04 cm)

Average wall thickness = 0.38 in. (0.96 cm)

Average height = 1.29 in. (3.28 cm)

The rings were tested in pairs, and their critical currents were measured by the pulsed-current facility at ANL. Typical test results are reported here.

Figure 9 shows a schematic diagram of the experimental apparatus. It consists of several capacitors in parallel and an array of field effect transistors (FETs). The capacitors are charged by a high-voltage DC current source (HVDC). The FETs are driven by a function generator, and the gates of the FETs can open and close in microseconds, which is much shorter than the transient time of the current experiments.

Figure 10 shows a schematic diagram of the test section. A copper coil is wound on the outside of the superconductor ring pair. The copper coil has 200 turns and is connected electrically to the pulsed current supply shown in Fig. 9. A Hall probe is placed near the center of the superconductor ring pair to measure the magnetic field at the center of the rings. A Rogowski coil measures the induced current in the superconductor rings. The voltage output of the Rogowski coil is proportional to the rate of change of the current threading through the loop formed by the Rogowski coil. Integrating the voltage with respect to time yields the net current. The induced current in the superconductor tube is obtained by subtracting the net current from the current through the copper coil measured by the precision resistor. The entire test section is kept at 77 K by submersion in liquid nitrogen in an open dewar.

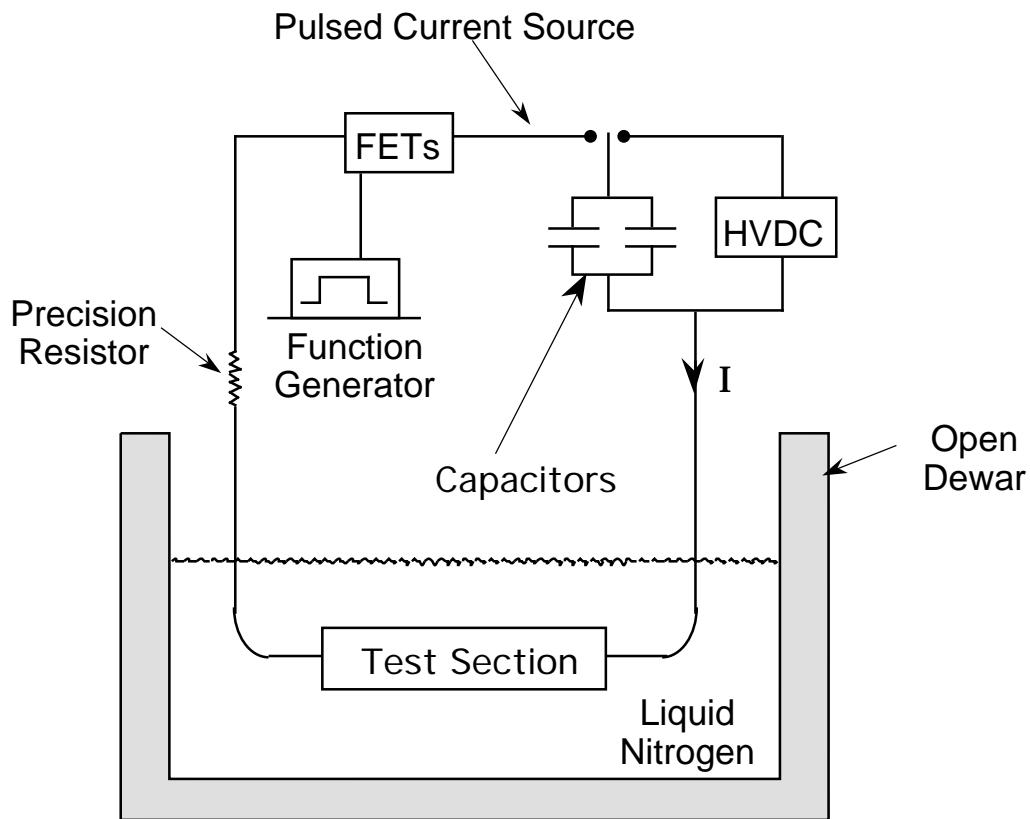


Fig. 9. Experimental apparatus for pulsed-current tests for measuring the critical currents of melt-textured YBCO rings.

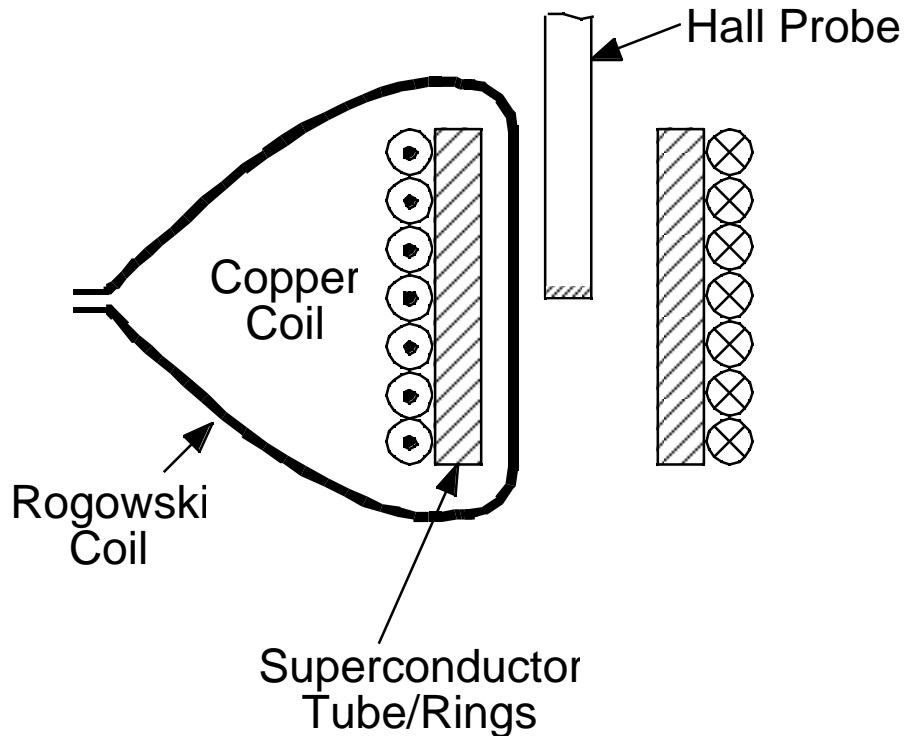


Fig. 10. Schematic diagram of the test section used to measure the critical currents of melt-textured YBCO rings.

Figures 11 to 13 show typical test results. In these figures,  $N$  is the number of turns of the copper coil,  $I$  is the pulsed current in the copper coil,  $H$  is the magnetic field strength measured by the Hall probe, and  $I(\text{ring})$  is the induced current in the superconductor ring pair, derived from the signal of the Rogowski coil. At relatively low excitation current (Fig. 11 with  $NI_{\text{max}} = 20,000$  A-turns), the peak-induced current in the superconductor rings was 15,000 A and was in the opposite direction of the excitation current. The difference between  $NI$  and  $I(\text{ring})$  is the result of magnetic flux leakage of the copper coil (not a long solenoid). The magnetic field  $H$  measured by the Hall probe shows a time delay of about 15 ms between  $NI_{\text{max}}$  and  $H_{\text{max}}$ . This delay is the result of magnetic diffusion, as is explained in references [1-3]. As the excitation current is increased (Fig. 12 with  $NI_{\text{max}} = 32,000$  A-turns), the time delay between  $NI_{\text{max}}$  and  $H_{\text{max}}$  decreases to about 11 ms, and the maximum induced current in the superconductor rings increases to 20,500 A. As the excitation current is further increased (Fig. 13 with  $NI_{\text{max}} = 48,000$  A-turns), the shielding capability (critical current) of the superconductor ring pair is reached, and the applied magnetic field penetrates the ring pair about 9 ms after the start of the current pulse.

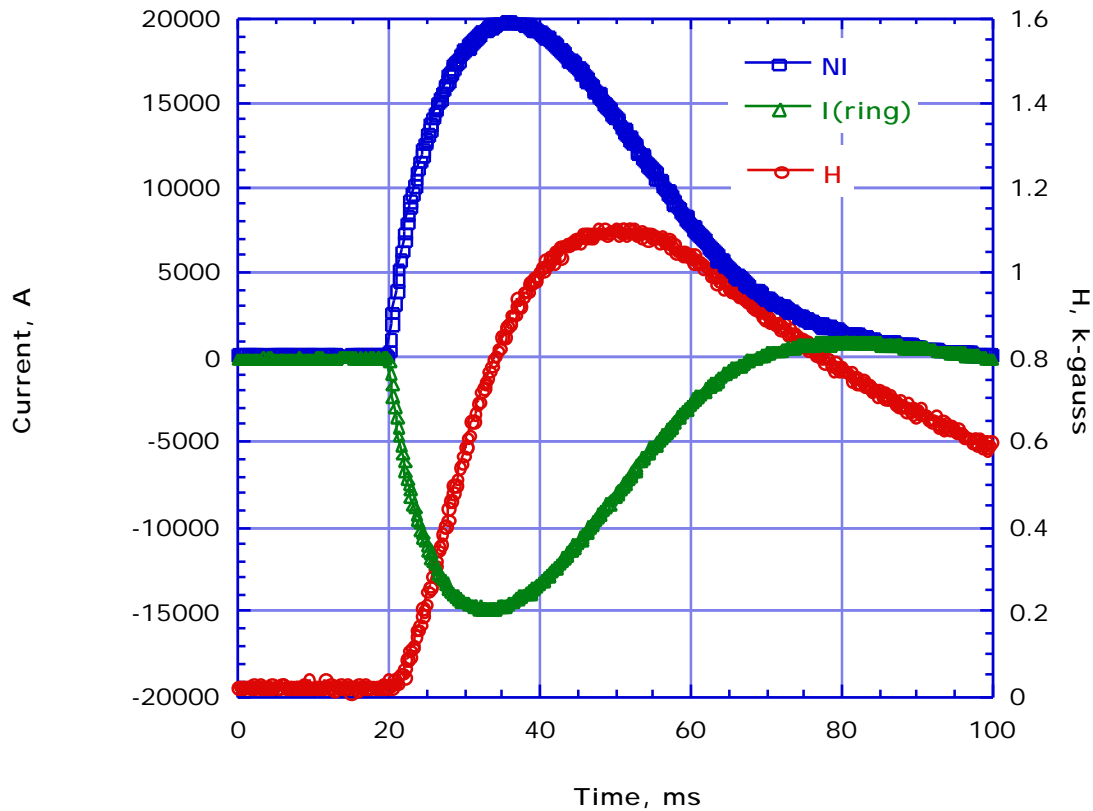


Fig. 11. Variations of the excitation current,  $NI$ , the magnetic field strength in the center of the YBCO rings,  $H$ , and the induced current in the YBCO rings,  $I(\text{ring})$ , versus time with  $NI_{\text{max}} = 20,000$  A-turns.

The results in Fig. 13 exhibit several distinct characteristics. At the instant of field penetration, the excitation current  $NI$  decreases slightly with time before it rises again, because the impedance of the test section suddenly increases when the applied magnetic field penetrates the superconductor rings. At the same instant of field penetration, there is a slope change of the magnetic field  $H$  inside the superconductor rings. This occurs because the Hall probe is sensing the magnetic field generated directly, instead of through magnetic diffusion, from the current in the coil after the rings are penetrated magnetically by the applied field. Because the applied field has penetrated the superconductor rings, the delay between  $NI_{\text{max}}$  and  $H_{\text{max}}$  should disappear, as confirmed in Fig. 13. Finally, at the instant of field penetration, the induced current in the rings,  $I(\text{ring})$ , begins to drop sharply as a result of heat dissipation in the superconductor rings. The maximum induced current in the rings seems to level off just before the instant at field penetration. This stabilization indicates maximum in the induced current should correspond to the critical current of the rings.

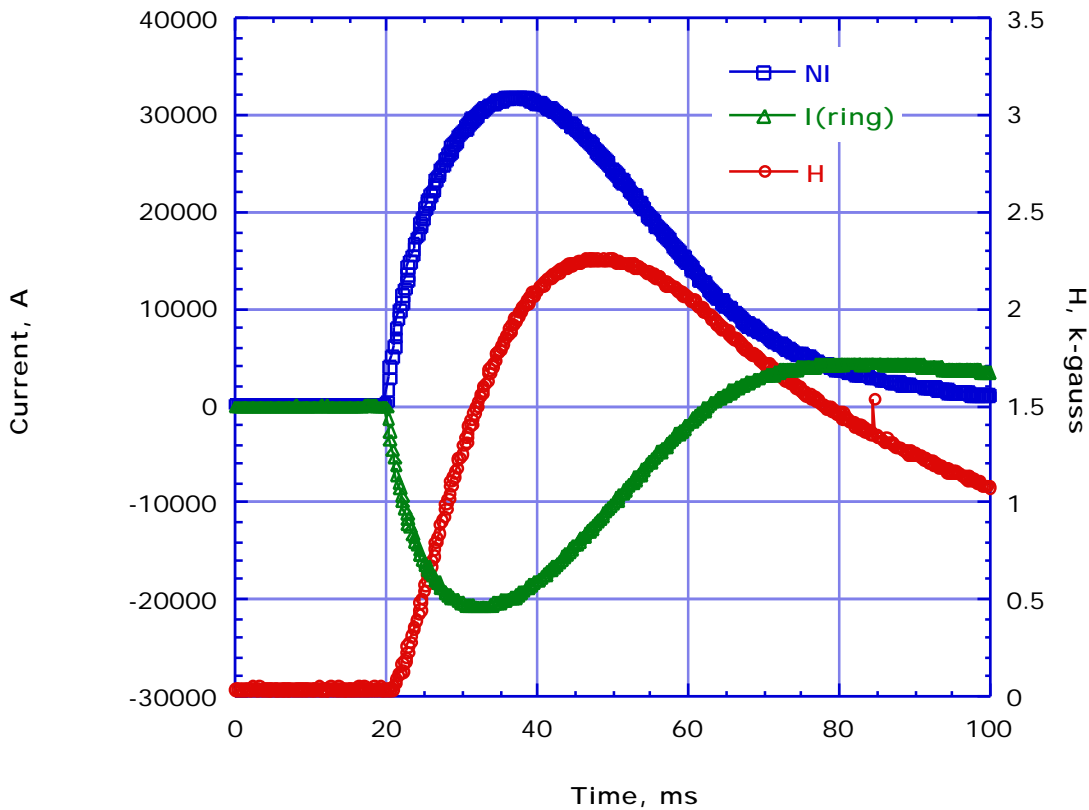


Fig. 12. Variations of the excitation current,  $NI$ , the magnetic field strength in the center of the YBCO rings,  $H$ , and the induced current in the YBCO rings,  $I(\text{ring})$ , versus time with  $NI_{\text{max}} = 32,000$  A-turns.

From Fig. 13, the critical current of the ring pair is 26,000 A; therefore, the average critical current of one ring is 13,000 A. Note that the critical current measured here is the critical current under pulsed conditions, which is much higher than that under AC steady-state conditions. Under AC steady-state conditions, more heat is dissipated in the superconductor, and this heat loss reduces the critical current significantly.

### References

1. Y. S. Cha and T. R. Askew, "Transient Response of a High-Temperature Superconductor Tube to Pulsed Magnetic Fields," *Physics C*, 32, 57-66, 1998.
2. Y. S. Cha, "Magnetic Diffusion in High- $T_c$  Superconductors," *Physica C*, 330, 1-8, 2000.
3. Y. S. Cha, "Magnetic Diffusion and Dissipation in High- $T_c$  Superconductors Subjected to Sinusoidal Applied Fields," *Physica C*, 361, 1-12, 2001.

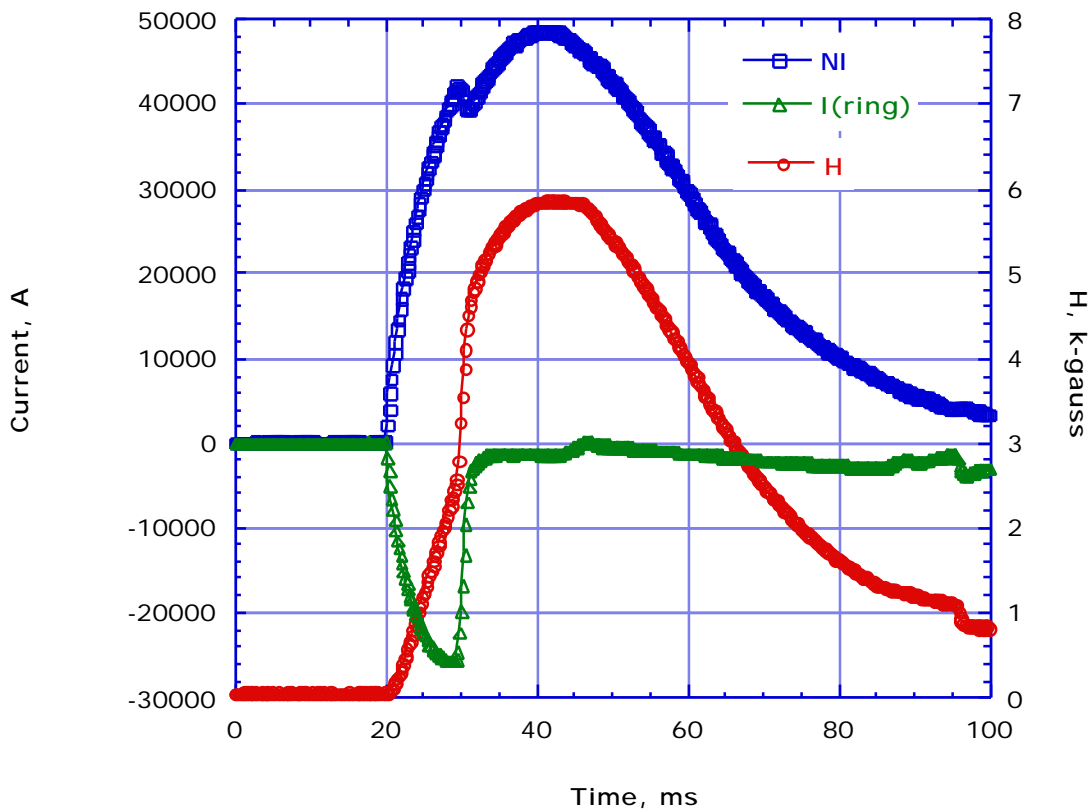


Fig. 13. Variations of the excitation current,  $NI$ , the magnetic field strength in the center of the YBCO rings,  $H$ , and the induced current in the YBCO rings,  $I(\text{ring})$ , versus time with  $NI_{\text{max}} = 48,000$  A-turns.

### Interactions

Balu Balachandran had programmatic discussion with DOE program managers in Washington, DC on Jan. 15, 2002.

Balu Balachandran visited IGC-SuperPower on January 18, 2002 and reviewed the HTSC program.

Steve Dorris, Beihai Ma, Victor Maroni, Dean Miller, and Balu Balachandran attended the DOE Wire Workshop in St. Petersburg, FL, Jan. 22-23, 2002.

On Feb. 14, 2002, Prof. Ted Van Duzer (University of California, Berkeley) visited Argonne and gave a colloquium on electronic application of superconductors.

Balu Balachandran visited IGC-SuperPower on Feb. 21, 2002 to review their program.

Balu Balachandran had programmatic discussion with DOE program managers in Washington, DC on March 12, 2002.

Balu Balachandran attended the International Superconductivity Industry Summit (ISIS-10) in Santa Fe, NM, March 15-16, 2002.

John Hull and Balu Balachandran attended the Applied Superconductivity Conference (ASC-2002) program committee meeting in Houston, TX, March 23-24, 2002, and helped to arrange the technical program for the upcoming ASC conference.

John Hull worked with the flywheel team at Boeing (Seattle, WA) on January 7-18, 2002.

## **Publications and Presentations**

### Published/Presented:

B. C. Prorok, J.-H. Park, K. C. Goretta, U. Balachandran; and M. M. McNallan (U. of Illinois at Chicago), Oxygen Diffusion Behavior During Internal Oxidation of Mg in Ag/1.12 at.% Mg, *Physica C* 370 (2002) 31-38.

B. Ma, M. Li, Y. A. Jee, R. E. Koritala, B. L. Fisher, and U. Balachandran, Inclined-Substrate Deposition of Biaxially Textured Magnesium Oxide Thin Films for YBCO Coated Conductors, *Physica C* 366 (2002) 270-276.

V. Vasanthamohan, T. B. Peterson, J. P. Singh, V. K. Vlasko-Vlasov, U. Welp, M. T. Lanagan, and G. W. Crabtree, Effect of Core Inhomogeneity on Strain Tolerance of Bi-2223 Composite Conductors, *Supercond. Sci. Technol.* 15 (2002) 94-98.

K. E. Gray, The Phenomenology of High-Temperature Superconductive Materials, Paper presented at the Space Technology and Applications Intl. Forum (STAIF-2002), 19th Symp. on Space Nuclear Power and Propulsion, Albuquerque, Feb. 3-7, 2002.

### Submitted:

M. Li, B. Ma, R. E. Koritala, B. L. Fisher, S. E. Dorris, V. A. Maroni, and U. Balachandran, Growth and Properties of YBCO Thin Films on Polycrystalline Ag Substrates by Inclined Substrate Laser Ablation, Submitted to *Superconductor Science and Technology*.

B. Ma, M. Li, B. L. Fisher, and U. Balachandran, Ion-Beam-Assisted Deposition of Biaxially Aligned Ytria-Stabilized Zirconia Template Films on Metallic Substrates for YBCO-Coated Conductors, Submitted to Superconductor Science and Technology (March 2002).

L. Chen, H. Claus, A. P. Paulikas, H. Zheng, and B. W. Veal, Joining of Melt-Textured YBCO: A Direct Contact Method, Paper to be presented at the Intl. Workshop on the Processing and Applications of Superconducting (RE)BCO Large Grain Materials, Seattle, July 11-13, 2002.

R. E. Koritala, B. Ma, M. Li, B. L. Fisher, U. Balachandran, and D. J. Miller, Texture Development of MgO Buffer Layers Grown by Inclined Substrate Deposition, Abstract to be presented at the Applied Superconductivity Conf., Houston, TX, Aug. 4-9, 2002.

B. Ma, M. Li, B. L. Fisher, R. E. Koritala, R. A. Erck, S. E. Dorris, and U. Balachandran, Biaxially Aligned Template Films Fabricated by Inclined-Substrate Deposition for YBCO-Coated Conductor Applications, Abstract to be presented at the Applied Superconductivity Conf., Houston, TX, Aug. 4-9, 2002.

Y. S. Cha, An Empirical Correlation for Electrical Field Strength of a Melt-Cast-Processed BSCCO-2212 Superconductor, Abstract to be presented at the Applied Superconductivity Conf., Houston, TX, Aug. 4-9, 2002.

T. R. Askew, J. M. Weber (Kalamazoo College); Y. S. Cha, H. Claus, and B. V. Veal, Transient Response of Single-Domain Y-Ba-Cu-O Rings to Pulsed Magnetic Fields, Abstract to be presented at the Applied Superconductivity Conf., Houston, Aug. 4-9, 2002.

S. Hanany (U. of MN), J. R. Hull, and Ki Ma (Texas Center for Superconductivity), Use of Superconducting Bearings to Measure Cosmic Microwave Background and Its Polarization, Abstract to be presented at the Applied Superconductivity Conf., Houston, Aug. 4-9, 2002.

### **2000-2002 Patents**

Method of manufacturing a high temperature superconductor with improved transport properties

Uthamalingam Balachandran, Richard Siegel, and Thomas Askew

U.S. Patent No. 6,191,075 (February 20, 2001).

Method and apparatus for measuring gravitational acceleration utilizing a high temperature superconducting bearing

John R. Hull

U.S. Patent 6,079,267 (June 27, 2000).

Method for preparing high temperature superconductor

Uthamalingam Balachandran and Michael P. Chudzik

U.S. Patent No. 6,361,598 (March 26, 2002).

Thermomechanical means to improve critical current density of BSCCO tapes

Uthamalingam Balachandran, Roger B. Poeppel, Pradeep Haldar (IGC), and Lesizek Motowidlo (IGC)

U.S. Patent 6,240,619 (June 5, 2001).

Bearing design for flywheel energy storage using high- $T_c$  superconductors

John R. Hull and Thomas M. Mulcahy

U.S. Patent No. 6,153,958 (Nov. 28, 2000).

Shielded high- $T_c$  BSCCO tapes or wires for high field applications

Uthamalingam Balachandran, Milan Lelovic, and Nicholas G. Eror

U.S. Patent No. 6,253,096 (June 26, 2001).